ACS OMEGA

Article

Cite This: ACS Omega 2018, 3, 2018−2026

Tetracarboxylate Linker-Based Flexible Cu^{II} Frameworks: Efficient Separation of CO_2 from CO_2/N_2 and C_2H_2 from C_2H_2/C_2H_4 Mixtures

Sohini Bhattacharyya, Anindita Chakraborty, Arpan Hazra, and Tapas Kumar Maji*

Molecular Materials Laboratory, Chemistry and Physics of Materials Unit, Jawaharlal Nehru Centre for Advanced Scientific Research, Bangalore 560064, India

Supporting Information

ABSTRACT: We report the synthesis, structure, and adsorption properties of two new metal−organic frameworks (MOFs) $\{[Cu_2(bpp)_3(\mathbf{L1})]\cdot(bpp)\cdot(4H_2O)\}$ (**1**) and $\{[Cu_2(bipy)_2(\mathbf{L2})\text{-}(H_2O)_2]\cdot(bipy)\cdot(5H_2O)\}$ (**2**) obtained from two different flexible tetracarboxylate linkers (**L1** and **L2**) of variable lengths and flexibility. While **1** comprising Cu^{II}, **L1**, and 1,3-bis(4-pyridyl) propane (bpp) is a 2D MOF with a cage-type structure, **2** consisting of Cu^{II}, **L2**, and 4,4′-bipyridine (bipy) has a 3D twofold interpenetrated structure. Both frameworks manifest permanent porosity, as realized from CO_2 adsorption at 195 K. **2** shows excellent CO_2/N_2 and C_2H_2/C_2H_4 adsorption selectivity at 298 K. This has been established by using **2** as a separating medium in a breakthrough column for separating mixtures of CO_2/N_2 (15:85, v/v) and C_2H_2/C_2H_4 (1:99, v/v). The selectivity of **2** toward CO_2 over N_2 and C_2H_2 over C_2H_4 is governed by favorable thermodynamic interactions owing to its structural flexibility, unsaturated metal sites, and polar carboxylate groups. Thus, **2** proves to be an extremely efficient material for specific gas separation.

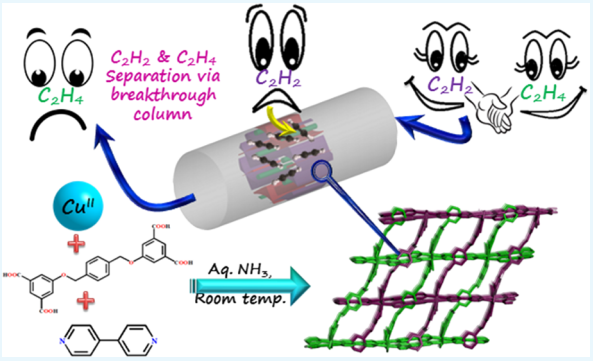

INTRODUCTION

Adsorptive separation[1] of a particular gas from a mixture using porous materials is a technique of supreme importance in recent times because of its relevance in industrial as well as environmental applications.[2,3] Different gas molecules are essential to sustain life[4] as well as to cater to our various energy requirements.[5] Thus, the effective sieving of the different components of a gas mixture is of paramount importance.[6] Hydrocarbons, particularly ethylene obtained from natural and shale gases, are extremely important in the polymer industry and to produce several other chemicals. During steam cracking for the synthesis of ethylene, acetylene (about 1%) is usually produced as a side product. This trace amount of acetylene is a contaminant which, if not removed, acts as a catalyst poison in ethylene polymerization and degrades the quality of the resultant polyethylene.[7] Thus, the development of porous materials which can facilitate selective adsorption of acetylene over ethylene is of paramount importance as it can show a cost-effective facile route for the challenging task of gas separation,[7−9] thereby helping the polymer industry immensely.

Metal−organic frameworks (MOFs),[10] well-known for their multifaceted applications in gas storage,[2,52] catalysis,[11] luminescence,[12] and sensing properties,[13,14] are extremely relevant in this regard. MOFs are much more efficient, both in terms of energy and cost, than traditional methods for gas separation, for example, cryogenic distillation or partial hydrogenation. Selectivity in MOFs can be achieved by tuning its pore size by modulating the functionalities of the organic linker along with implementation of suitable metal ions with varied geometry.[15−17] By controlling the window dimension or pore size of MOFs, kinetic-based separation can be achieved.[2,18,19] Also, separation can be done on the basis of favorable thermodynamic interaction of the specific adsorbate molecules with the pore surface.[8,20,21] Thus, it is extremely important to adopt a proper targeted ligand design strategy to synthesize such MOFs with high efficiency. Multidentate flexible linkers, for example, di, tri, and tetra carboxylates,[24−27,51] are the most widely used linkers in MOF chemistry.[22,23] Such linkers coordinate with metal ions to form a wide range of multinuclear nodes with predictable geometries such as binuclear paddle-wheel units, tri, or tetranuclear units.[25] In this regard, aromatic tetracarboxylate linkers are particularly utilitarian because of the more number of coordinating sites as well as the rich π-electron density.[25,27] MOFs constructed from such π-electron-rich tetracarboxylate ligands have pore surfaces studded with a large number of oxygen atoms providing better interactions with gas molecules such as CO_2[28,29] or small hydrocarbon molecules such as ethylene and acetylene.[30,31] Furthermore, the flexibility of such ligands contributes to the tunable porosity of MOFs by inducing guest-responsive structural dynamicity[23,31,32,50] with

Received: December 9, 2017
Accepted: January 30, 2018
Published: February 19, 2018

DOI: 10.1021/acsomega.7b01964
ACS Omega 2018, 3, 2018−2026

Scheme 1. pH-Dependent Synthesis of Compounds 1 and 2 by the Self-Assembly of Cu^{II} and Respective Linkers at Room Temperature

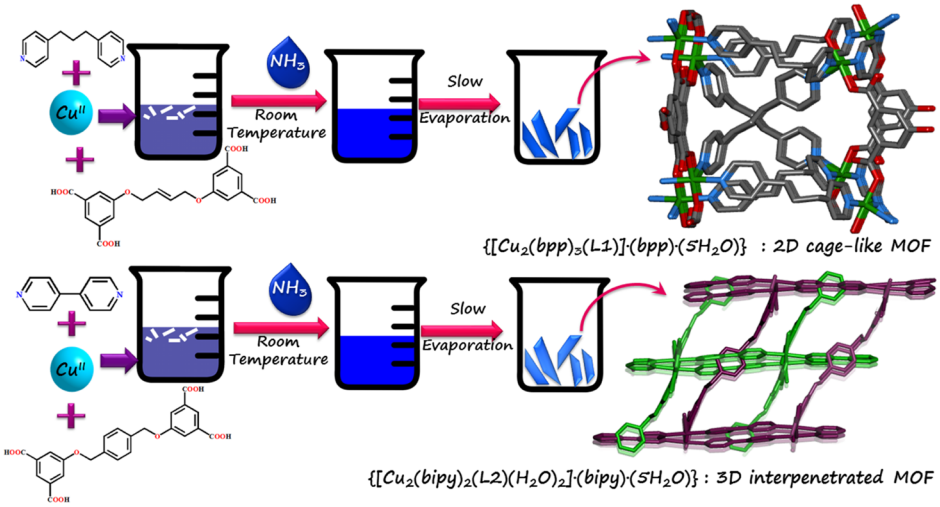

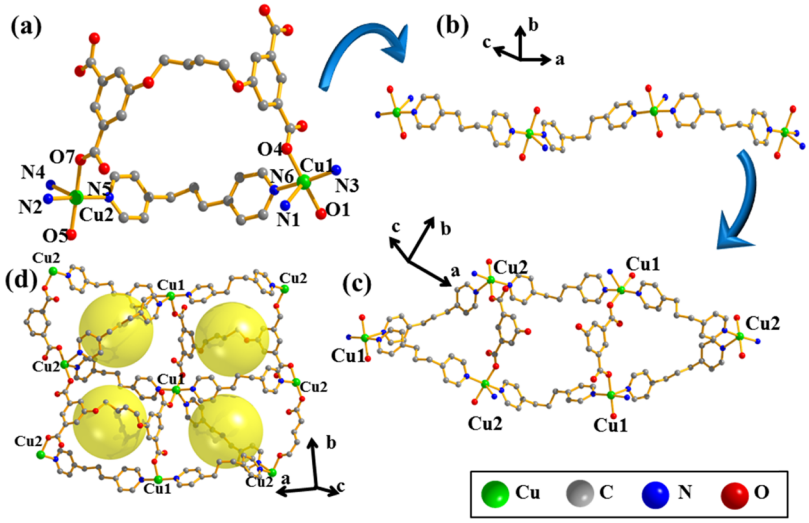

Figure 1. (a) Coordination sphere of Cu1 and Cu2 in compound **1**. (b) 1D wavy chain of **1** formed by Cu centers linked with bpp molecules. (c) 2D network in **1**. (d) Hydrophobic pockets in the framework.

the ability to respond to external stimuli,[33] for example, temperature, pressure, light, electric fields, and chemical inclusion.[11,32] Such dynamic frameworks[34] also manifest stepwise[35] or gated adsorption[36,37] at a certain pressure of an adsorbate molecule[38,39] which results in guest selectivity[31,40] and gas separation.[40−42]

In this work, we have used two different flexible tetracarboxylate π-electron-rich linkers [5,5′-(1,4-(2-butene)-bis(oxy)diisophthalic acid (**L1**) and 5,5′-(1,4-phenylenebis-(methylene))bis(oxy)diisophthalic acid (**L2**) (Scheme 1) of different lengths and flexibility. Self-assembly of **L1** and 1,3-bis(4-pyridyl) propane (bpp) with Cu^{II} at room temperature results in a hydrophobic 2D MOF $\{[Cu_2(bpp)_3(\mathbf{L1})]\cdot(bpp)\cdot(4H_2O)\}$ (**1**) (CCDC no. 1590169) with a cage[43]-type structure. The permanent porosity of the framework has been established by performing CO_2 adsorption at 195 K by different vapor adsorption studies. On the other hand, self-assembly of **L2** and bipyridine (bipy) with Cu^{II} resulted in a twofold interpenetrated 3D MOF $\{[Cu_2(bipy)_2(\mathbf{L2})(H_2O)_2]\cdot(bipy)\cdot(5H_2O)\}$ (**2**) (CCDC no. 1590168). The desolvated framework (**2′**) exhibits an excellent selectivity toward C_2H_2 over C_2H_4 at 298 K, the practical applicability of which has been proven using a breakthrough column experiment. Additionally, it is also a selective adsorbent of CO_2 from its mixture with N_2, making it a potential material for the separation for industrial flue gas. In both cases, the basis of separation is the favorable thermodynamic interaction of the framework with respective adsorbate molecules.

RESULTS AND DISCUSSION

Description of the Crystal Structure of Compounds 1 and 2. Single-crystal X-ray diffraction (SCXRD) data reveal that compound **1** crystallizes in a monoclinic $P2_1/c$ space group. The asymmetric unit contains two crystallographically independent penta-coordinated Cu^{II} centers that have a (4 + 1) square pyramidal geometry. The degree of deviation from ideal square pyramidal geometry has been calculated in terms of Addison parameter (τ),[44] the value of which is merely 0.019 for Cu1, suggesting a square pyramidal geometry rather than a trigonal bipyramid. The basal plane of Cu1 is occupied by N3 and N6 from two different bpp linkers along with two carboxylate oxygen atoms O1 and O4 from two different **L1**

DOI: 10.1021/acsomega.7b01964
ACS Omega 2018, 3, 2018−2026

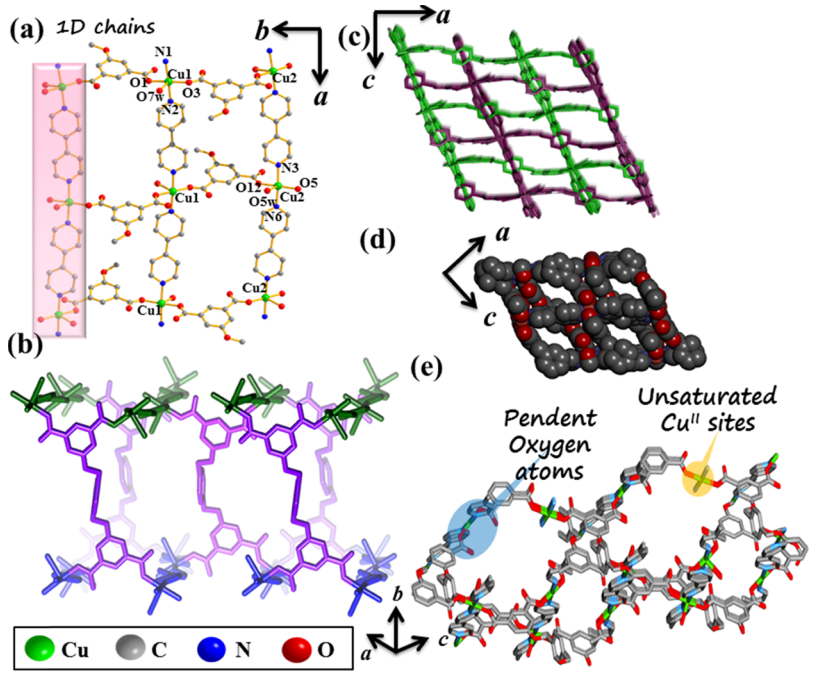

Figure 2. (a) 2D sheet viewed along the crystallographic *c* direction in **2**. (b) 3D network of **2**. (c) 3D two- fold interpenetrated framework of **2**. (d) Pore structure in **2**. (e) Pendent oxygen atoms and unsaturated Cu^{II} sites on the pore surface of **2**.

linkers. The apical position is occupied by the N1 atom from another bpp ligand (Figure 1a). The Cu1−O1 bond length at the basal plane is 1.93(8) Å, whereas that for Cu1−O4 is 1.97(8) Å. The bond lengths for Cu1−N3 and Cu1−N6 are 2.03(10) and 2.04(14) Å, respectively. However, the Cu1−N1 bond at the apical position is much longer with a bond length of 2.32(10) Å, implying a (4 + 1) geometry. Similarly, the pentacoordination of Cu2 is fulfilled by two carboxylate oxygen atoms (O5 and O7) from **L1** and two nitrogen atoms (N4 and N5) from two different bpp linkers at the basal plane and N2 at the apical position (Figure 1a). The τ value for Cu2 is 0.13, suggesting high distortion from ideal square pyramidal geometry. The bond lengths of Cu2−O5 and Cu2−O7 are 1.97(10) and 1.94(9) Å, respectively, whereas those of Cu2−N4 and Cu2−N5 are 2.03(12) and 2.04(12) Å, respectively. The apical Cu2−N2 is much longer, with a bond length of 2.36(13) Å. Cu1 and Cu2 are connected together by a bpp linker to form a wavy chain (Figure 1b). Two such parallel chains are connected by an **L1** linker, where the two carboxylates at one terminal of **L1** connect two Cu1 atoms and the two carboxylates at the other terminal connect two Cu2 atoms (Figure 1d). Adjacent to this, the Cu1 center is further diagonally connected to a Cu2 atom in the other chain by a bpp linker. Thus, a 2D network with a cagelike structure is formed containing a hydrophobic pocket along the *b* direction (Figure 1d), which is lined by the π-electron-rich aromatic **L1** on one side and a bpp linker on the other. This hydrophobic pocket houses a guest bpp molecule which forms a $\pi-\pi$ interaction with the pyridyl ring of the bpp ligand on the wall of the pocket (cg−cg distance 4.6 Å). The central C3 alkyl moiety in the case of both **L1** as well as bpp imparts flexibility to the pockets, thereby ensuring uptake of adsorbate molecules in spite of the small pore size. All the guest water molecules present in the framework, except for O5w, are hydrogen-bonded with the framework. The hydrogen-bonding parameters of **1** have been summarized in Table S3. The solvent accessible void space in the framework is 2943.3 $Å^3$ (39.6% of the total cell volume), which has been calculated using PLATON after removing the guest bpp and the water molecules.

Compound **2** crystallizes in the *C*2/*c* monoclinic space group. Each asymmetric unit comprises two crystallographically independent pentacoordinated Cu^{II} centers, each of which assumes a distorted square pyramidal geometry, the degree of distortion being as low as 0.007 for Cu1 and 0.037 for Cu2. The pentacoordination of Cu1 is fulfilled by two nitrogen atoms (N1 and N2) from two different bipy molecules, two oxygen atoms (O1 and O3) from tetracarboxylate linker **L2**, and one coordinated water molecule (O7w). Similarly, the pentacoordination of Cu2 is satisfied by two nitrogen atoms (N3 and N6) from two different bipy linkers, two oxygen atoms (O5 and O12) from **L2**, and one oxygen atom (O5w) from a coordinated water molecule. The bipy linker (containing N6 and N7 atoms), connecting two adjacent Cu2 centers, is disordered over two positions with 50−50 equal occupancy (Figure S5a). Cu1 centers connected by bipy linkers form a 1D chain along the *a* direction, and a similar 1D chain is formed by the bridging of Cu2 centers by bipy along the crystallographic *a* direction (Figure 2a). The two carboxylates on one terminal of an **L2** linker (marked in violet in Figure 2b) connect two of these parallel chains on one plain (marked in dark green in Figure 2b). The two carboxylates on the other terminal of the **L2** connect two other such parallel 1D chains on a different plain (marked in blue in Figure 2b) to form the 3D framework (Figure 2c). Two 3D frameworks interpenetrate each other, resulting in a twofold interpenetrated 3D framework (Figure 2d). Along the crystallographic *b* direction, the single nets of the 3D framework contain a 1D channel with a pore dimension of 4.45 × 5.46 $Å^2$, which upon twofold interpenetration (Figures 2c and S3b) reduces to a smaller channel having a pore dimension of 2.93 × 5.14 $Å^2$, and the channel is occupied by guest bipy and guest water molecules. Detailed analysis with TOPOS[48,49] reveals that compound **2** is the 5-nodal (2-c)(4-

DOI: 10.1021/acsomega.7b01964
ACS Omega 2018, 3, 2018−2026

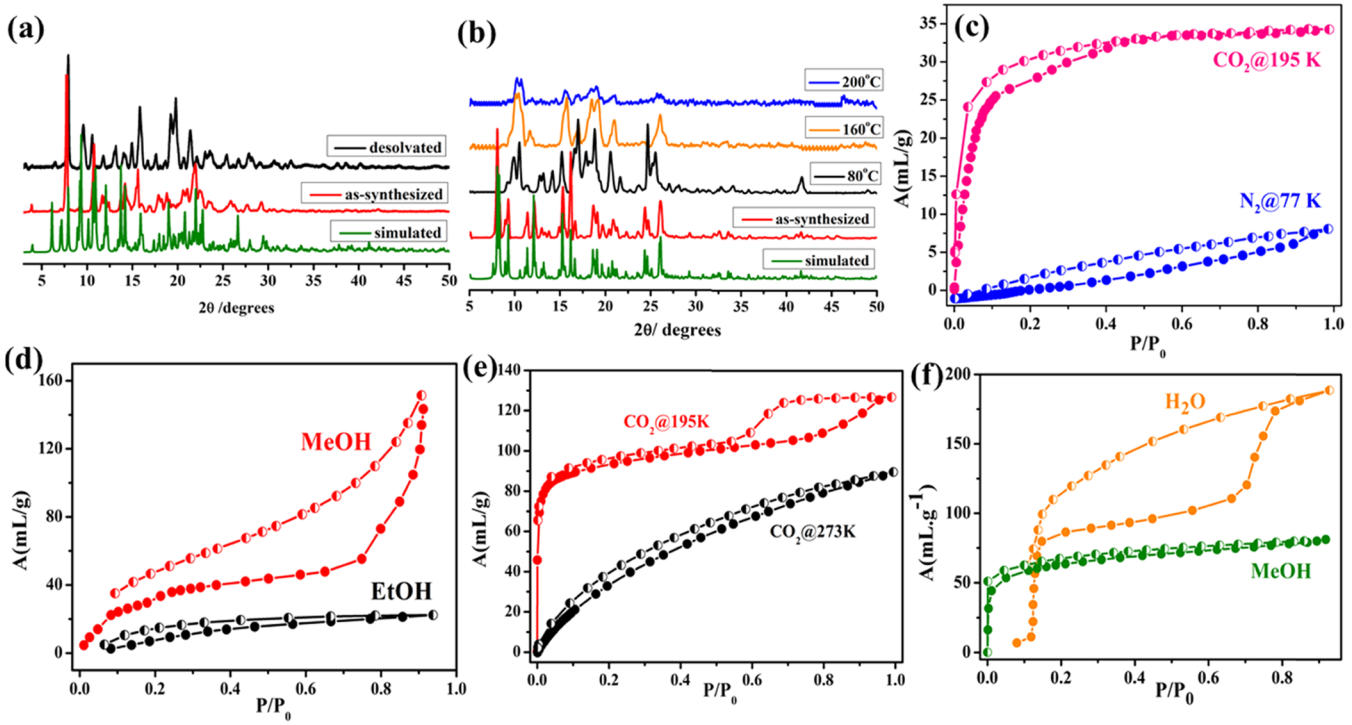

Figure 3. (a) PXRD pattern of **1** in different states. (b) PXRD pattern of **2** with the increasing temperature. (c) CO_2 and N_2 adsorption isotherms of compound **1**. (d) Solvent adsorption isotherms of compound **1**. (e) CO_2 adsorption isotherm of **2′** at 195 and 273 K. (f) Solvent adsorption isotherms of **2′**.

c)$_2$(4-c)$_2$ periodic net connected by two 4-connected (4-c) Cu centers, by two 4-connected (4-c) **L2** ligands, and one 2-connected (2-c) bipy ligand. Further analysis shows that compound **2** adopts an unprecedented network topology with the Schlafli symbol $\{6^2.7^2.8.9\}_2\{6^3.7.8^2\}\{6^4.8.9\}\{6^4.8^2\}^2\{7\}$. All the water molecules, except O4w, are hydrogen-bonded to the framework, and the hydrogen bonding parameters have been summarized in Table S6. The pyridyl ring (containing the N4 atom) of guest bipy molecules shares a $\pi-\pi$ interaction (cg−cg distance 3.76 Å) with the pyridyl ring (containing the N1 atom) of bipy linkers along the pore wall. As we have discussed earlier, both Cu1 and Cu2 are coordinated to water molecules, and thus, unsaturated metal sites (UMS) could be generated after desolvation. The solvent accessible void is 5826.1 Å^3 (47.5% of the total cell volume) and has been calculated using PLATON after removing the coordinated and as well as guest water and guest bipy molecules.

Framework Stability and PXRD. The thermogravimetric analysis (TGA) of compound **1** shows an initial loss of ∼4%, corresponding to three guest water molecules (Figure S6a). Subsequently, there is a continuous weight loss beyond ∼150 °C which may be attributed to the loss of the remaining two guest water molecules and the guest bpp molecule, which can be explained on the basis of SCXRD analysis. Two of the guest water molecules are released at higher temperature. Beyond 200 °C, the framework degrades continuously.

The powder X-ray diffraction (PXRD) pattern of the as-synthesized compound **1** matches perfectly with the simulated pattern, suggesting the phase purity (Figure 3a). The framework on being desolvated undergoes structural changes, as evident from the PXRD pattern of the framework desolvated at 135 °C under vacuum (10^{-1} Pa). On desolvation, there is rearrangement in the Bragg's reflections, along with peak broadening and appearance of new peaks, suggesting a structural transformation.

The TGA of **2** shows an initial loss of ∼9% up to 100 °C owing to the loss of all 5 guest water molecules and one of the coordinated water molecules (Figure S6a). The subsequent ∼13% loss starting at 140 °C can be attributed to the loss of the second coordinated water molecule and guest bipyridine molecules. The desolvated framework degrades almost continuously beyond this.

The PXRD pattern of the as-synthesized compound **2** is in accordance with the simulated pattern. The structure of compound **2** shows changes with the increasing temperature, as evident from the desolvated PXRD pattern (Figure 3b). This can be attributed to the removal of the coordinated water molecules and the guest bipy molecules, which interact with the framework via $\pi-\pi$ stacking. The removal of the bipy molecule gives rise to another structural phase. In this framework, along with guest water molecules, there are coordinated water molecules, and their removal results in the generation of UMS. Such a change in the coordination sphere of the Cu^{II} center ensues structural changes, as reflected from the PXRD pattern.

Gas and Solvent Vapor Adsorption. Although compound **1** does not have a definite pore in any direction, the presence of a pocket lined by electron rich aromatic benzene and pyridine rings along the crystallographic *b* direction (Figure 1d) prompted us to check the adsorption behaviour of the desolvated compound (**1′**). At 195 K, the adsorption isotherm of **1′** shows an uptake of 35 mL g^{-1} CO_2, with a steep uptake in the low-pressure region. This can be attributed to the interaction of the CO_2 molecules with the free pendant carboxylate oxygen atoms flanking the pore surface and the π-electron density on the pore surface from the aromatic rings of the ligand (Figure 3c). The water adsorption curve (Figure

DOI: 10.1021/acsomega.7b01964
ACS Omega 2018, 3, 2018−2026

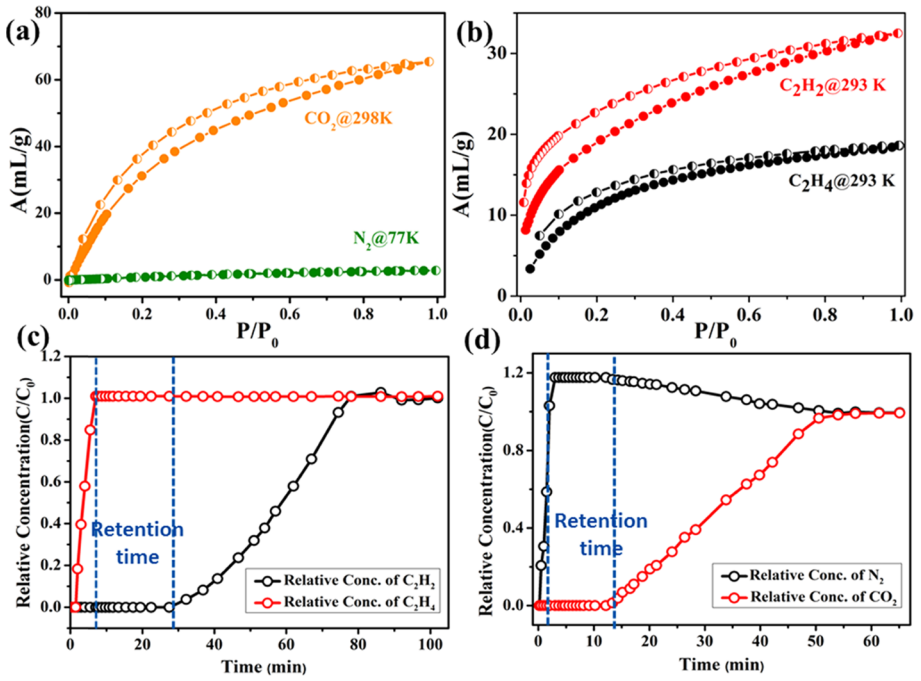

Figure 4. (a) CO_2 adsorption isotherm at 298 K and N_2 at 77 K for **2′**. (b) Adsorption isotherms for C_2H_2 and C_2H_4 at 293 K for **2′**. Breakthrough curves for a binary mixture of (c) N_2/CO_2 (0.85:0.15) and (d) C_2H_2/C_2H_4 (0.1:0.99) for **2′**.

S7a) confirms the hydrophobic nature of the framework exhibiting poor uptake at lower pressures, which is also reiterated in the MeOH and EtOH adsorption isotherms (Figure 3d). The net adsorption amount decreases from water (2.7 Å) to methanol (3.6 Å) to ethanol (4.5 Å) as the kinetic diameter of the solvent molecules increase in that order. The lower polarity of MeOH ensures a steeper uptake at low pressures, as compared to water, but the net uptake of water is much higher owing to its smaller size. Although the hydrophobic MOF is expected to show a good adsorption of nonpolar solvents such as benzene, the small pore dimensions of **1** restrict the adsorption of benzene (kinetic diameter of benzene being 5.9 Å) (Figure S7a).

To check the porous properties of compound **2**, the N_2 adsorption isotherm of the desolvated framework (**2′**) was measured at 77 K. **2′** does not adsorb N_2, which is attributed to the high-diffusion barrier of the inert N_2 gas (kinetic diameter: 3.65 Å) in the narrow channel of **2′** (2.93 × 5.14 $Å^2$ along the *b* direction) (Figure 2d). Moreover, the accessible void space in this framework is very small because of the twofold interpenetration. However, framework **2′** manifests an appreciable amount of CO_2 uptake at 195, 273, as well as at 298 K. At 195 K, **2′** records the adsorption of 127 mL g^{-1} CO_2, with a steep uptake in the low-pressure region, indicating its microporous nature (Figure 3e). Steps are observed at various stages of adsorption, which manifest that the framework is flexible in nature, and there are different adsorption sites for CO_2. Desorption does not follow the same path as adsorption initially, and we observe a hysteresis till P/P_0 = 0.55, below which both the curves converge. The adsorption amount of CO_2 is 85 mL g^{-1} at 273 K and 65 mL g^{-1} at 298 K. **2′** shows type-I adsorption at 298 K where the adsorption and desorption curves do not coincide, exhibiting a narrow hysteretic profile (Figure 3e). Besides the pendant oxygen atoms on the pore surface, the presence of UMS, that is, pentacoordinated Cu^{II} centers, along the pore further contributes to the enhanced adsorption (Figure 2e). Also, the kinetic diameter of CO_2 is smaller (3.64 Å), and its high quadruple moment interacts with the π-electron cloud of the aromatic rings on the pore surface. The polar hydrophilic nature of the pore surface of **2′** is manifested by the solvent adsorption profiles (Figures 3f and S5b). The adsorption isotherms of CO_2 at 273 and 298 K were fitted in the virial equation, from which the isosteric heat of adsorption ($Q_{st,f}$) for **2′** was calculated to be ∼18.9 kJ mol^{-1} at the zero coverage region (Figure S10b).[8]

Intrigued by this, we proceeded to predict the selectivity of **2′** toward CO_2 over N_2 at 298 K using the Clausius−Clapeyron equation. At 298 K for **2′**, the predicted ideal adsorbed solution theory (IAST)[45] selectivities of CO_2 over N_2 for a bimolar (0.15:0.85) mixture of CO_2−N_2 is 13. Also here, the selectivity increases with the increasing pressure. At pressure 101 kPa, the CO_2−N_2 selectivity is 94 (Figure S9a).

Such a good theoretical value prompted us to check the actual separation ability of **2** for CO_2 gas from a binary CO_2/N_2 (0.15:0.85) mixture at room temperature (293 K). Tightly packed columns of **2′** (400 mg, column length 4 cm) were prepared and activated with a He gas (flow rate 1 mL/min). The breakthrough curve of the binary mixture of CO_2/N_2 (0.15:0.85) for **2′** is represented in Figure 4c, where it exhibits a CO_2 retention time of 11 min. This high retention time indicates that **2′** holds immense potential for practical use as a medium for separating CO_2 from other gases.

Inspired by such efficiency of **2′** in separating CO_2 and N_2, we were further interested in exploiting the flexible structure and UMS for C2 [acetylene (C_2H_2) and ethylene (C_2H_4)] hydrocarbon storage and separation. Thus, **2′** was checked for C_2H_2 and C_2H_4 adsorption, and it was found that **2′** can adsorb 38 mL g^{-1} C_2H_2 at 273 K, whereas the adsorption amount for C_2H_4 is 27 mL g^{-1} at 273 K (Figure S8). **2′** shows a steeper uptake of C_2H_2 at lower pressure, as compared to C_2H_4. At P/P_0 = 0.01, the adsorbed amount of C_2H_2 per gram of **2′** is 11.5

DOI: 10.1021/acsomega.7b01964
ACS Omega 2018, 3, 2018−2026

mL when the adsorbate is C_2H_2, whereas that for C_2H_4 is merely 5 mL. The desorption curve for C_2H_2 takes a different route than the adsorption isotherm, thereby forming a hysteresis, indicating a strong interaction between the framework and C_2H_2. At 293 K, the adsorption amounts are 33 mL g^{-1} for C_2H_2 (Figure 4b) and 16 mL g^{-1} for C_2H_4. The isosteric heat of adsorption calculated for C_2H_2 is 32 kJ mol^{-1} at the zero coverage region (Figure S8d,e). Thus, because of a higher Q_{st} value, C_2H_2 attains more accessibility to the pore surface and interacts with the UMS, unlike C_2H_4. At 293 K, the predicted selectivity of C_2H_2 over C_2H_4 for a (0.01:0.99) mixture of the two gases is calculated in a similar manner as for CO_2−N_2, using IAST,[45] which is 3.7 initially, and the selectivity decreases gradually with increasing pressure (Figure S9b). Thus, the easy accessibility to UMS coupled with good IAST selectivity, high room-temperature uptake, and relatively low heat of adsorption certifies that **2′** is an ideal material for C_2H_2−C_2H_4 separation.

To establish the practical applicability of **2** in separating a trace amount of C_2H_2 from C_2H_4, we performed an actual breakthrough experiment where we fed a column of **2′** with a (1:99, v/v) mixture of C_2H_2 and C_2H_4 at 298 K. Interestingly, C_2H_4 appears within a few seconds of starting the gas flow. The breakthrough time for C_2H_2 is 27 min (Figure 4d). This is a rather unique feat achieved by any MOF at room temperature and aptly upholds the efficiency of **2** in real-time applications.

CONCLUSIONS

In conclusion, two different flexible tetracarboxylate ligands **L1** and **L2** have been successfully implemented in two different frameworks, **1** and **2**, along with other linkers. The variable flexibility and the aromatic π-electron-rich nature of the ligands impart very interesting properties within the framework. The presence of a hydrophobic pocket, lined by aromatic rings from the ligand in compound **1**, enables it to adsorb a reasonable amount of CO_2 at 195 K. On the other hand, compound **2**, with a 3D framework with twofold interpenetration, is a promising adsorbent material owing to the presence of the polar carboxylate groups, UMS, and flexible structure. It shows a good IAST selectivity toward C_2H_2 over C_2H_4, which is culminated in practical applications using a breakthrough column. **2′** can retain C_2H_2 for a very long time within this breakthrough column, releasing pure C_2H_4. Moreover, **2′** also manifests excellent CO_2−N_2 separation. The selectivity of CO_2 over N_2 and C_2H_2 over C_2H_4 is attributed to more favorable thermodynamic interactions. Thus, frameworks constructed from such tetracarboxylate ligands can be used as effective materials for specific gas sequestration and separation by tuning flexibility and functionalities.

EXPERIMENTAL SECTION

Materials. All the reagents and solvents were used as obtained from commercial supplies without any further purification. Dimethyl-5-hydroxy isophthalate, α,α'-dibromo-paraxylene, dibenzo-18-crown-6, 1,4-dibromobutene, and K_2CO_3 were obtained from Aldrich Co. Ltd.

Synthesis of {[Cu_2(bpp)$_3$(L1)]·(bpp)·(4H_2O)} (1). $CuCl_2$·$2H_2O$ (0.2 mmol, 0.034 g) and solid **L1** (0.1 mmol, 0.047 g) were mixed with 10 mL of water and stirred for 10 min. Aqueous ammonia (20%) was added dropwise to this mixture till the solution becomes clear. To this, 10 mL methanolic solution of 1,3-bis(4-pyridyl)propane (0.5 mmol, 0.099 g) was added, and the resulting solution was stirred for 1 h. The solution was kept undisturbed at room temperature. After 3−4 days, dark blue needle-shaped crystals appear. Yield: 60% relative to Cu^{II}. Anal. Calcd for $C_{12}H_{17}Cu_2N_{17}$: C, 61.051; H, 5.123; and N, 7.910%. Found: C, 60.99; H, 5.43; and N, 7.72%. FT-IR (4000−400 cm^{-1}) 1568 (s), 1618 (s), 1358 (s), and 778 (s) cm^{-1}.

Synthesis of {[Cu_2(bipy)$_2$(L2)(H_2O)$_2$]·(bipy)·(5H_2O)} (2). $CuCl_2$·$2H_2O$ (0.2 mmol, 0.034 g) and solid **L1** (0.1 mmol, 0.047 g) were mixed with 20 mL of water and stirred for 10 min. Aqueous ammonia (20%) was added dropwise to this reaction mixture until the solid residues dissolve, and the solution becomes clear. Subsequently, a 10 mL methanolic solution of 4,4′-bipyridine (0.5 mmol, 78 mg) was added to the previous reaction mixture, and the solution was stirred overnight. The solution was kept undisturbed at room temperature. Light blue crystals are formed after 3−4 days. Yield: 72% relative to Cu^{II}. Anal. Calcd. for $C_{54}H_{46}Cu_2N_6O$: C, 55.054; H, 3.935; and N, 7.133%. Found: C, 55.26; H, 3.45; and N, 7.27%. FT-IR (4000−400 cm^{-1}) 782 (s), 1265 (s), 1354 (s), 1570 (s), 1616 (s), and 3900 (w) cm^{-1}.

For characterization and adsorption studies, phase pure single crystals were used.

Physical Measurements. The elemental analyses were carried out using a Thermo Fischer FLASH 2000 elemental analyzer. IR spectra were recorded with a Bruker IFS 66v/S spectrophotometer using KBr pellets in the region of 4000−400 cm^{-1}. TGA was carried out (Mettler Toledo) in a nitrogen atmosphere (flow rate = 50 mL/min) in the temperature range of 30−500 °C (heating rate = 3 °C min^{-1}). PXRD patterns of the compounds in different states were recorded by using Cu Kα radiation (Bruker D8 DISCOVER; 40 kV, 30 mA).

X-ray Crystallography. X-ray single-crystal structural data for **1** and **2** were collected using a Bruker SMART-CCD diffractometer equipped with a normal focus and a 2.4 kW sealed tube X-ray source with graphite monochromated Mo Kα radiation (λ = 0.71073 Å) operating at 50 kV and 30 mA. The program SAINT[14] was used for integration of diffraction profiles, and absorption correction was made using the SADABS[15] program. All of the structures were solved using SHELXT[47] and refined by a full matrix least square method using SHELXL-2017.[46] All of the hydrogen atoms were geometrically fixed and placed in ideal positions. The potential solvent accessible area or void space was calculated using the PLATON multipurpose crystallographic software.[18] All crystallographic and structure refinement data for **1** and **2** are summarized in Table 1. Selected bond lengths and angles for **1** and **2** are given in Tables S1−S6, respectively.

Adsorption Study. The adsorption isotherms of CO_2 (195, 273 and 298 K) and N_2 (77 K, 298 K), and other gases (C_2H_2 and C_2H_4 at 273 and 298 K) using the desolvated sample of **1** (**1′**) and **2** (**2′**) were measured by using a Quantachrome Autosorb IQ2 analyzer. In the sample tube adsorbent, samples **1** and **2** (~100−150 mg) were placed which had been prepared at 353 and 433 K, respectively, under a 1×10^{-1} Pa vacuum for about 6 h prior to the measurement of the isotherms. Helium gas (99.999% purity) at a certain pressure was introduced in the gas chamber and allowed to diffuse into the sample chamber by opening the valve. The amount of gas adsorbed was calculated readily from the pressure difference ($P_{cal} - P_e$), where P_{cal} is the calculated pressure with no gas adsorption and P_e is the observed equilibrium pressure. All operations were computer-controlled and automatic.

DOI: 10.1021/acsomega.7b01964
ACS Omega 2018, 3, 2018−2026

Table 1. Crystal Data and Structure Refinement Parameters for Compounds 1 and 2

parameter	1	2
empirical formula	$C_{72}H_{72}Cu_2N_8O_{15}$	$C_{54}H_{46}Cu_2N_6O_{17}$
formula weight	1398.4	1177.9
crystal system	monoclinic	monoclinic
space group	$P2_1/c$ (no. 14)	$C2/c$ (no. 15)
a, Å	23.6727(17)	44.8511(10)
b, Å	18.9130(13)	19.0460(4)
c, Å	17.6128(13)	14.7115(3)
β, deg	109.696(3)	102.380(1)
V, Å^3	7424.6	12 274.8
Z	4	8
T, K	293	293
μ, mm^{-1}	0.638	0.766
D_{calcd}, g/cm^3	1.249	1.331
$F(000)$	2904	5072
reflections $[I > 2\sigma(I)]$	3751	6004
unique reflections	8042	9461
measured reflections	94 274	81 471
R_{int}	0.171	0.085
GOF on F^2	0.96	1.03
$R_1[I > 2\sigma(I)]^a$	0.1040	0.068
$R_w[I > 2\sigma(I)]^b$	0.2956	0.2170

$^aR = \sum||F_0| - |F_c||/\sum|F_0|$ $^bR_w = [\sum\{w(F_0^2 - F_c^2)^2\}/\sum\{w(F_0^2)^2\}]^{1/2}$.

The adsorption of different solvents such as MeOH at 293 K and H_2O and EtOH at 298 K was measured in the desolvated sample of **1** and **2** in the vapor state by using a BELSORP Aqua-3 analyzer. The samples of about ∼100−150 mg were activated under similar conditions as mentioned earlier. The different solvent molecules used to generate the vapor were degassed fully by repeated evacuation. The dead volume was measured with helium gas. The adsorbate was placed into the sample tube, and then the change of pressure was monitored and the degree of adsorption was determined by the decrease in pressure at the equilibrium state. All operations were computer-controlled and automatic.

Breakthrough Measurements. Breakthrough experiments were performed using a column (packed with about 400 mg of powdered **2′**), 4 cm long in length and 0.3 cm in diameter. The sample was first activated at 160 °C for 12 h prior to loading in the column. After loading, the sample was again activated with the He flow for 30 min. CO_2/N_2 (v/v 15:85 mixture) and C_2H_2/C_2H_4 (v/v 1:99 mixture) streams were passed through the column with He. The flow was continuous, and the flow rate was regulated by a Mass Flow Controller (MFC). The partial pressure of the gas mixture was kept at p = 5 kPa. The gas stream at the outlet of the column was analyzed on-line with gas chromatography. The space velocity was kept at 4.71 min^{-1} (Figure S11).

■ ASSOCIATED CONTENT

Supporting Information

The Supporting Information is available free of charge on the ACS Publications website at DOI: 10.1021/acsomega.7b01964.

Detailed ligand synthesis, associated data, and details of the breakthrough experiment setup and other calculations (PDF)

Crystal data for compound **1** (CIF)

Crystal data for compound **2** (CIF)

■ AUTHOR INFORMATION

Corresponding Author

*E-mail: tmaji@jncasr.ac.in (T.K.M.).

ORCID

Anindita Chakraborty: 0000-0001-5109-3890

Tapas Kumar Maji: 0000-0002-7700-1146

Notes

The authors declare no competing financial interest.

■ ACKNOWLEDGMENTS

S.B. is grateful to INSPIRE Fellowship, Department of Science and Technology, Govt. of India, for fellowship. T.K.M. thanks Sheikh Saqr Laboratory for Single Crystal X-ray Diffraction facilities. T.K.M. is grateful to the Department of Science and Technology (DST, project no. MR-2015/001019 and project no. TRC-DST/C.14.10/16-2724, JNCASR), Govt. of India and JNCASR for financial support.

■ REFERENCES

(1) Chen, L.; Reiss, P. S.; Chong, S. Y.; Holden, D.; Jelfs, K. E.; Hasell, T.; Little, M. A.; Kewley, A.; Briggs, M. E.; Stephenson, A.; Thomas, K. M.; Armstrong, J. A.; Bell, J.; Busto, J.; Noel, R.; Liu, J.; Strachan, D. M.; Thallapally, P. K.; Cooper, A. I. Separation of rare gases and chiral molecules by selective binding in porous organic cages. *Nat. Mater.* **2014**, *13*, 954−960.

(2) Li, J.-R.; Kuppler, R. J.; Zhou, H.-C. Selective adsorption and separation in metal-organic frameworks. *Chem. Soc. Rev.* **2009**, *38*, 1477−1504.

(3) Kang, Z.; Fan, L.; Sun, D. Recent advances and challenges of metal-organic framework membranes for gas separation. *J. Mater. Chem. A* **2017**, *5*, 10073−10091.

(4) Zhang, W.; Banerjee, D.; Liu, J.; Schaef, H. T.; Crum, J. V.; Fernandez, C. A.; Kukkadapu, R. K.; Nie, Z.; Nune, S. K.; Motkuri, R. K.; Chapman, K. W.; Engelhard, M. H.; Hayes, J. C.; Silvers, K. L.; Krishna, R.; McGrail, B. P.; Liu, J.; Thallapally, P. K. Redox-Active Metal-Organic Composites for Highly Selective Oxygen Separation Applications. *Adv. Mater.* **2016**, *28*, 3572−3577.

(5) Li, B.; Wang, H.; Chen, B. Microporous metal-organic frameworks for gas separation. *Chem.−Asian J.* **2014**, *9*, 1474−1498.

(6) Banerjee, D.; Elsaidi, S. K.; Thallapally, P. K. Xe adsorption and separation properties of a series of microporous metal−organic frameworks (MOFs) with V-shaped linkers. *J. Mater. Chem. A* **2017**, *5*, 16611−16615.

(7) Hazra, A.; Jana, S.; Bonakala, S.; Balasubramanian, S.; Maji, T. K. Separation/purification of ethylene from an acetylene/ethylene mixture in a pillared-layer porous metal-organic framework. *Chem. Commun.* **2017**, *53*, 4907−4910.

(8) Li, L.; Lin, R.-B.; Krishna, R.; Wang, X.; Li, B.; Wu, H.; Li, J.; Zhou, W.; Chen, B. Efficient separation of ethylene from acetylene/ethylene mixtures by a flexible-robust metal-organic framework. *J. Mater. Chem. A* **2017**, *5*, 18984−18988.

(9) Hu, T.-L.; Wang, H.; Li, B.; Krishna, R.; Wu, H.; Zhou, W.; Zhao, Y.; Han, Y.; Wang, X.; Zhu, W.; Yao, Z.; Xiang, S.; Chen, B. Microporous metal-organic framework with dual functionalities for highly efficient removal of acetylene from ethylene/acetylene mixtures. *Nat. Commun.* **2015**, *6*, 7328.

(10) Kitagawa, S.; Kitaura, R.; Noro, S.-i. Functional Porous Coordination Polymers. *Angew. Chem., Int. Ed.* **2004**, *43*, 2334−2375.

(11) Liu, J.; Chen, L.; Cui, H.; Zhang, J.; Zhang, L.; Su, C.-Y. Application of metal-organic frameworks in heterogeneous supramolecular catalysts. *Chem. Soc. Rev.* **2014**, *43*, 6011−6061.

(12) Roy, S.; Chakraborty, A.; Maji, T. K. Lanthanide-organic frameworks for gas storage and as magneto-luminescent materials. *Coord. Chem. Rev.* **2014**, *273−274*, 139−164.

DOI: 10.1021/acsomega.7b01964
ACS Omega 2018, 3, 2018−2026

(13) Hu, Z.; Deibert, B. J.; Li, J. Luminescent metal-organic frameworks for chemical sensing and explosive detection. *Chem. Soc. Rev.* **2014**, *43*, 5815−5840.
(14) Horike, S.; Shimomura, S.; Kitagawa, S. Soft Porous Crystals. *Nat. Chem.* **2009**, *1*, 695−704.
(15) Dzubak, A. L.; Lin, L.-C.; Kim, J.; Swisher, J. A.; Poloni, R.; Maximoff, S. N.; Smit, B.; Gagliardi, L. Ab initio carbon capture in open site metal-organic frameworks. *Nat. Chem.* **2012**, *4*, 810−816.
(16) Duke, A. S.; Dolgopolova, E. A.; Galhenage, R. P.; Ammal, S. C.; Heyden, A.; Smith, M. D.; Chen, D. A.; Shustova, N. B. Active Sites in Copper-Based Metal-organic frameworks: Understanding Substrate Dynamics, Redox Processes, and Valence-Band Structure. *J. Phys. Chem. C* **2015**, *119*, 27457−27466.
(17) Easun, T. L.; Moreau, F.; Yan, Y.; Yang, S.; Schröder, M. Structural and dynamic studies of substrate binding in porous metal-organic frameworks. *Chem. Soc. Rev.* **2017**, *46*, 239−274.
(18) Park, H. J.; Suh, M. P. Stepwise and hysteretic sorption of N_2, O_2, CO_2 and H_2 gases in a porous metal-organic framework $[Zn_2(BPnDC)_2(bpy)]$. *Chem. Commun.* **2010**, *46*, 610−612.
(19) Yang, S.; Lin, X.; Lewis, W.; Suyetin, M.; Bichoutskaia, E.; Parker, J. E.; Tang, C. C.; Allan, D. R.; Rizkallah, P. J.; Hubberstey, P.; Champness, N. R.; Thomas, K. M.; Blake, A. J.; Schröder, M. A partially interpenetrated metal-organic framework for selective hysteretic sorption of carbon dioxide. *Nat. Mater.* **2012**, *11*, 710−716.
(20) Hazra, A.; Bonakala, S.; Bejagam, K. K.; Balasubramanian, S.; Maji, T. K. Host-guest [2+2] Cycloaddition Reaction: Postsynthetic Modulation of CO_2 selectivity and Magnetic Properties in a Bimodal Metal-organic framework. *Chem.—Eur. J.* **2016**, *22*, 7792−7799.
(21) Xiang, S.; He, Y.; Zhang, Z.; Wu, H.; Zhou, W.; Krishna, R.; Chen, B. Microporous metal-organic framework with potential for carbon dioxide capture at ambient conditions. *Nat. Commun.* **2012**, *3*, 954.
(22) Lin, Z.-J.; Lü, J.; Hong, M.; Cao, R. Metal-organic frameworks based on flexible ligands (FL-MOFs): structures and applications. *Chem. Soc. Rev.* **2014**, *43*, 5867−5895.
(23) Chang, Z.; Yang, D.-H.; Xu, J.; Hu, T.-L.; Bu, X.-H. Flexible Metal-organic Frameworks: Recent Advances and Potential Applications. *Adv. Mater.* **2015**, *27*, 5432−5441.
(24) Ling, Y.; Chen, Z.-X.; Zhai, F.-P.; Zhou, Y.-M.; Weng, L.-H.; Zhao, D.-Y. A zinc(II) metal-organic framework based on traizole and dicarboxylate ligands for selective adsorption of hexane isomers. *Chem. Commun.* **2011**, *47*, 7197.
(25) Lin, X.; Jia, J.; Zhao, X.; Thomas, K. M.; Blake, A. J.; Walker, G. S.; Champness, N. R.; Hubberstey, P.; Schröder, M. *Angew. Chem., Int. Ed.* **2006**, *45*, 7358.
(26) Wee, L. H.; Wiktor, C.; Turner, S.; Vanderlinden, W.; Janssens, N.; Bajpe, S. R.; Houthoofd, K.; Van Tendeloo, G.; De Feyter, S.; Kirschhock, C. E. A.; Martens, J. A. Copper Benzene Tricarboxylate Metal-organic Framework with Wide Permanent Mesopores Stabilized by Keggin Polyoxometallate Ions. *J. Am. Chem. Soc.* **2012**, *134*, 10911.
(27) Pan, Z.; Zheng, H.; Wang, T.; Song, Y.; Li, Y.; Guo, Z.; Batten, S. R. Hydrothermal Synthesis, Structures, and Physical Properties of Four New Multicarboxylate Ligands-Based Compounds. *Inorg. Chem.* **2008**, *47*, 9528−9536.
(28) Liu, J.; Thallapally, P. K.; McGrail, B. P.; Brown, D. R.; Liu, J. Progress in adsorption-based CO_2 capture metal-organic frameworks. *Chem. Soc. Rev.* **2012**, *41*, 2308−2322.
(29) Masoomi, M. Y.; Stylianou, K. C.; Morsali, A.; Retailleau, P.; Maspoch, D. Selective CO_2 Capture in Metal-organic Frameworks with Azine-functionalized Pores Generated by Mechanosynthesis. *Cryst. Growth Des.* **2014**, *14*, 2092−2096.
(30) Wu, S.; Ma, L.; Long, L.-S.; Zheng, L.-S.; Lin, W. Three-dimensional Metal-organic Frameworks Based on Functionalized Tetracarboxylate Linkers: Synthesis, Structures, and Gas Sorption Studies. *Inorg. Chem.* **2009**, *48*, 2436−2442.
(31) Mukherjee, S.; Joarder, B.; Desai, A. V.; Manna, B.; Krishna, R.; Ghosh, S. K. Exploiting Framework Flexibility of a Metal-organic Framework for Selective Adsorption of Styrene over Ethylbenzene. *Inorg. Chem.* **2015**, *54*, 4403−4408.
(32) Schneemann, A.; Bon, V.; Schwedler, I.; Senkovska, I.; Kaskel, S.; Fischer, R. A. Flexible Metal-organic frameworks. *Chem. Soc. Rev.* **2014**, *43*, 6062−6096.
(33) Kanoo, P.; Haldar, R.; Reddy, S. K.; Hazra, A.; Bonakala, S.; Matsuda, R.; Kitagawa, S.; Balasubramanian, S.; Maji, T. K. Crystal Dynamics in Multi-stimuli Responsive Entangled Metal-organic Frameworks. *Chem.—Eur. J.* **2016**, *22*, 15864−15873.
(34) Schneemann, A.; Takahashi, Y.; Rudolf, R.; Noro, S.-i.; Fischer, R. A. Influence of Co-adsorbates on CO2 induced phase transitions in functionalized pillared-layered metal-organic frameworks. *J. Mater. Chem. A* **2016**, *4*, 12963−12972.
(35) Sakaida, S.; Otsubo, K.; Sakata, O.; Song, C.; Fujiwara, A.; Takata, M.; Kitagawa, H. Crystalline coordination framework endowed with dynamic gate-opening behaviour by being downsized to a thin film. *Nat. Chem.* **2016**, *8*, 377−383.
(36) Bärwinkel, K.; Herling, M. M.; Rieß, M.; Sato, H.; Li, L.; Avadhut, Y. S.; Kemnitzer, T. W.; Kalo, H.; Senker, J.; Matsuda, R.; Kitagawa, S.; Breu, J. Constant Volume Gate-opening by Freezing Rotational Dynamics in Microporous Organically Pillared Layered Silicates. *J. Am. Chem. Soc.* **2017**, *139*, 904−909.
(37) Li, L.; Krishna, R.; Wang, Y.; Yang, J.; Wang, X.; Li, J. Exploiting the gate opening effect in a flexible MOF for selective adsorption of propyne from C1/C2/C3 hydrocarbons. *J. Mater. Chem. A* **2016**, *4*, 751−755.
(38) Kanoo, P.; Sambhu, R.; Maji, T. K. Guest-Specific Double- or Single-step Adsorption in a Flexible Porous Framework Based on a Mixed-ligand System. *Inorg. Chem.* **2011**, *50*, 400−402.
(39) Liu, B.; Li, Y.; Hou, L.; Yang, G.; Wang, Y.-Y.; Shi, Q.-Z. Dynamic Zn-based metal-organic framework: stepwise adsorption, hysteretic desorption and selective carbon dioxide uptake. *J. Mater. Chem. A* **2013**, *1*, 6535−6538.
(40) Mukherjee, S.; Joarder, B.; Manna, B.; Desai, A. V.; Chaudhari, A. K.; Ghosh, S. K. Framework-flexibility Driven Selective Sorption of *p*-Xylene over Other Isomers by a Dynamic Metal-organic Framework. *Sci. Rep.* **2014**, *4*, 5761.
(41) Haldar, R.; Reddy, S. K.; Suresh, V. M.; Mohapatra, S.; Balasubramanian, S.; Maji, T. K. Flexible and Rigid Amine-Functionalized Microporous Frameworks Based on Different Secondary Building Units: Supramolecular Isomerism, Selective CO_2 Capture and Catalysis. *Chem.—Eur. J.* **2014**, *20*, 4347−4356.
(42) Foo, M. L.; Matsuda, R.; Hijikata, Y.; Krishna, R.; Sato, H.; Horike, S.; Hori, A.; Duan, J.; Sato, Y.; Kubota, Y.; Takata, M.; Kitagawa, S. An Adsorbate Discriminatory Gate Effect in a Flexible Porous Coordination Polymer for Selective Adsorption of CO_2 over C_2H_2. *J. Am. Chem. Soc.* **2016**, *138*, 3022−3030.
(43) Lan, Y.-Q.; Jiang, H.-L.; Li, S.-L.; Xu, Q. Mesoporous Metal-organic Frameworks with Size-tunable Cages: Selective CO_2 Uptake, Encapsulation of Ln^{+3} Cations for Luminescence and Column-Chromatographic Dye Separation. *Adv. Mater.* **2011**, *23*, 5015−5020.
(44) Addison, A. W.; Rao, T. N.; Reedijk, J.; van Rijn, J.; Verschoor, G. C. Synthesis, structure and spectroscopic properties of copper(II) containing nitrogen-sulphur donor ligands; the crystal and molecular structure of aqua[1,7-bis(N-methylbenzimidazol-2′-yl)-2,6-dithiaheptane]copper(II) perchlorate. *J. Chem. Soc., Dalton Trans.* **1984**, 1349−1356.
(45) Myers, A. L.; Prausnitz, J. M. Thermodynamics of mixed-gas Adsorption. *AlChE J.* **1965**, *11*, 121−127.
(46) Sheldrick, G. M. *SHELXL 97, Program for the Solution of Crystal Structure*; University of Göttingen: Germany, 1997.
(47) *S. V. a. SMART (V 5.628), XPREP, SHELXTL*; Bruker AXS Inc.: Madison, Wisconsin, USA, 2004.
(48) Blatov, V. A.; Carlucci, L.; Ciani, G.; Proserpio, D. M. Interpenetrating metal-organic and inorganic 3D networks: a computer-aided systematic investigation. Part I. Analysis of cambridge structural database. *CrystEngComm* **2004**, *6*, 377−395.
(49) Blatov, V. A.; Shevchenko, A. P.; Serezhkin, V. N. TOPOS3.2: a new version of the program package for multipurpose crystal-chemical analysis. *J. Appl. Crystallogr.* **2000**, *33*, 1193.

DOI: 10.1021/acsomega.7b01964
ACS Omega 2018, 3, 2018−2026

(50) Vishnoi, P.; Kaleeswaran, D.; Kalita, A. Ch.; Murugavel, R. Dependence of the SBU length on the size of metal ions in akaline earth MOFs derived from C_3-symmetric tricarboxylic acid. *CrystEngComm* **2016**, *18*, 9130−9138.
(51) Halder, A.; Bhattacharya, B.; Haque, F.; Ghoshal, D. Structural Diversity in Six Metal Ligand Zn(II) Metal-organic Frameworks Constructed by Rigid and Flexible Dicarboxylates and Different N,N′Donor Ligands. *Cryst. Growth Des.* **2017**, *17*, 6613−6624.
(52) Sharma, V.; De, D.; Saha, R.; Das, R.; Chattaraj, P. K.; Bharadwaj, P. K. A Cu(II)-MOF capable of fixing CO_2 from air and showing high capacity H_2 and CO_2 adsorption. *Chem. Commun.* **2017**, *53*, 13371−13374.

DOI: 10.1021/acsomega.7b01964
ACS Omega 2018, 3, 2018−2026